Editors' Suggestion

Pair filamentation and laser scattering in beam-driven QED cascades

Kenan Qu,* Alec Griffith, and Nathaniel J. Fisch
Department of Astrophysical Sciences, Princeton University, Princeton, New Jersey 08544, USA

(Received 4 December 2023; accepted 19 January 2024; published 27 March 2024)

We report the observation of longitudinal filamentation of an electron-positron pair plasma in a beam-driven QED cascade. The filaments are created in the "pair-reflection" regime, where the generated pairs are partially stopped and reflected in the strong laser field. The density filaments form near the center of the laser pulse and have diameters similar to the laser wavelength. They develop and saturate within a few laser cycles and do not induce sizable magnetostatic fields. We rule out the onset of two-stream instability or Weibel instability and attribute the origin of pair filamentation to laser ponderomotive forces. The small plasma filaments induce strong scattering of laser energy to large angles, serving as a signature of collective QED plasma dynamics.

DOI: 10.1103/PhysRevE.109.035208

I. INTRODUCTION

The global race to build ultrastrong lasers worldwide [1–3] has brought us closer to laboratory testing of strong-field QED effects [4–6]. Although directly producing the Schwinger field, $E_{cr} \sim 10^{18}\,\mathrm{Vm}^{-1}$, remains obscure, different schemes [7–14] to magnify the impact of existing technologies have been proposed. The most promising technique [7,8] involves the collision of an ultrastrong laser pulse with a highly energetic electron beam, boosting the field by a large Lorentz factor in the rest frame of the electron beam to reach the Schwinger limit. This method was adopted in the seminal QED experiment at SLAC [15,16] to yield measurable electron-positron pairs. Similar experiments have been enabled by the development of the laser-wakefield accelerator, which recently reported exploring the quantum radiation reaction using petawatt (PW) lasers and GeV electron beams generated by the laser [17,18]. If the charge in the electron beam can be increased to the nC level using, e.g., a conventional electron accelerator, its collision with multi-PW laser is predicted to create a QED plasma [19–28].

QED plasma is a state that describes the interplay of both strong-field QED effect and collective plasma dynamics. It plays a key role in extreme astrophysical environments and in experiments using next generation Schwinger-level high power lasers. Thus, validating the QED theory is crucial notwithstanding the significant challenges associated with generating sufficiently dense electron-positron pairs. Multiple criteria exist to define the threshold where dense pairs transition into a pair plasma. It's noteworthy that collective effects can manifest in dilute plasmas even if its dimension is shorter than the Debye length and plasma skin depth, as highlighted by Stenson *et al.* [29]. In the context of laser-plasma interaction, plasma effects become important when the plasma frequency constitutes a substantial percent of laser frequency. Indeed, QED PIC simulations [23,24] demonstrate that creation of pair plasma in the laser field leads to an observable upshift of laser frequency and the amount of frequency upshift is dependent on the plasma frequency [30–33]. The laser frequency upshift arises from the change in the plasma dispersion relation, which is generally considered as governing the electromagnetic plasma mode.

In this paper, we focus on the spatial properties of the simulation and report observations of pair plasma filamentation and large-angle laser scattering. Pair density filamentation emerges in the "pair reflection" regime. This regime is achieved when the laser intensity reaches the threshold value, $I_{th} = 10^{22}-10^{23}\,\mathrm{Wcm}^{-2}$, which is sufficient to slow down and stop the created pair particles through the combined effects of radiation reaction and laser ponderomotive force. When the created pairs are temporarily stopped, they exhibit the lowest Lorentz factor and thus the maximum plasma frequency. The highly inhomogeneous plasma, characterized by a scale comparable the laser wavelength, induces Mie scattering. The scattered light undergoes intensity modulation at different scattering angles, leading to an expulsion of pairs toward low-intensity regions. Simultaneously, the laser is refracted toward regions with low plasma density. These coupled processes induce the ponderomotive filamentation instability [34–37]. This instability, recognized as one of the fastest growing modes [38,39] in relativistic plasma streams, is amplified by the reduction of pair slippage rate with the laser pulse, facilitated by pair reflection. Because the pair filaments are automatically aligned with the laser peak, they continuously scatter the laser toward higher angles, causing a quick decrease in peak laser intensity. The coherent scattered light, stemming from laser-plasma interaction, serves as another signature of QED plasma effects. The flexibility of detecting the scattering at large off-axis angles reduces the experimental complexity.

This paper explains the pair filamentation instability through the analysis of results from a 3D QED PIC simulation. The details of the simulation parameters are presented in Sec. II. The section also describes the evolution of pair filaments, including the pair density, distribution function, and the corresponding magnetic fields. The dynamics of laser pulse is presented in Sec. III, in which we provide an

*Corresponding author: kq@princeton.edu

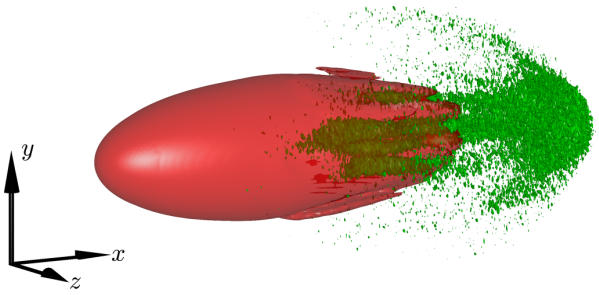

FIG. 1. Pair filamentation (green) and laser scattering (red) as a result of e^--beam driven QED cascade. The laser is polarized in the y direction and propagates to the $+x$ direction. The e^- beam (not shown) propagates to the $-x$ direction. The snapshot is taken at $t = 0.22$ ps.

analytical estimation of the laser intensity decrease. Finally, we present in Sec. IV our conclusions and discuss the implication of QED plasma experiments.

II. FORMATION OF PAIR FILAMENTATION

The pair filaments are observed in 3D QED PIC simulations that we described in Refs. [23,24]. A snapshot of the laser beam and created pairs are plotted in Fig. 1 to show the simulation schematics. The simulations consider collision of a 300 GeV electron beam and a 24 PW laser pulse. The electron beam has 1 nC charge distributed in a Gaussian sphere with rms radius of 1 μm. Its peak density is 4×10^{20} cm^{-3}. The Gaussian laser pulse has $\lambda = 0.8$ μm wavelength, 6×10^{22} Wcm^{-2} peak intensity (correspondingly $a_0 \approx 170$), 50 fs rms duration, and 5 μm waist. The laser is linearly polarized in the y direction and propagates to the $-x$ direction. The electron beam propagates to the $+x$ direction. The numerical parameters are similar to those in Ref. [23], but we increase the transverse simulation window size to $(40\,\mu\text{m})^2$ to capture the pair expansion. The transverse grid size is correspondingly increased to $(\lambda/6)^2$.

The electrons have a maximum quantum parameter $\tilde{\chi}_e \approx 220$ at the Gaussian waist in the focal plane, and $\tilde{\chi}_e \approx 600$ at the laser focus. The high quantum parameter $\tilde{\chi}_e$ enables a beam-driven QED cascade which creates electron positron pairs through the Breit-Wheeler process. The stochastic nature leads to a broad distribution function of the pair momentum with higher creation probability for lower pair energy. Importantly, the low energy pairs play the dominant role in collective plasma dynamics because a more detailed description of the QED cascade can be found in Ref. [24]. As the pairs continue to lose energy through radiation reaction, those in the low energy spectrum begin to become reflected by the ponderomotive pressure assuming that the laser intensity exceeds the "pair reflection" threshold [23,26]. Thus, we can divide the pair evolution into three stages, including forward moving, being stopped, and being reflected. All the pairs at different stages can coexist but the pairs in each stage contain both electrons and positrons moving in the same longitudinal direction, making the plasma quasineutral and anisotropic.

The pair plasma, illustrated in green in Fig. 1, exhibits filamentation in the region where it overlaps with the laser

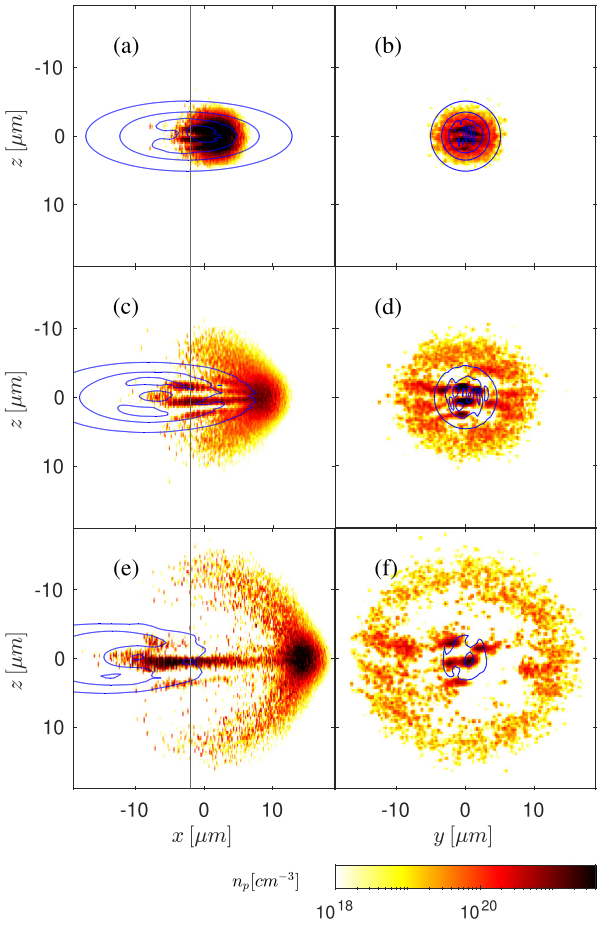

FIG. 2. Pair density (cm^{-3}) at $t = 0.18$ ps (a), (b), 0.2 ps (c), (d), and 0.22 ps (e), (f), respectively. The blue curves show the laser intensity contours at $1, 3, 5, 7 \times 10^{22}$ Wcm^{-2} from outer to inner, respectively. The left column shows the $y = 0$ cross section and the right column shows the $x = -2$ μm cross section indicated by the vertical line on the left.

pulse. To show more details of the filaments, we plot in Fig. 2 the evolution of pair density profile and the laser intensity contours in the $x - z$ plane at $y = 0$ (left column) and the $y - z$ plane at $x = -2$ μm (right column). Although the simulation is conducted in a 100 μm-long box, we only show the center part where pair density is finite. Pairs are created with a total charge of 139 nC and peak density of $n_p \approx 3 \times 10^{22}$ Wcm^{-2}. They initially have a spherical profile similar to the injected electron beam. The sphere then expands under the laser radiation pressure and develops density fringes as shown in Fig. 2(b).

With decreasing pair energy, the plasma frequency $\omega_p \propto \sqrt{n_p/\gamma}$ continues to grow. Its peak value is reached when the majority of pairs reach the "pair reflection" condition, which is shown in Fig. 2(a) as cavitation of the pair sphere at $t = 0.2$ ps. The laser field also shows distortion when propagating through the dense plasma. The maximum plasma frequency corresponds to a skin depth $c/\omega_p \approx 12$ μm. The

fringes condense into filaments and gain a wave vector in the y direction, which can be seen in Fig. 2(d). As the same time, the cavitation continues to expand. The pair plasma develops three structures, including a dense core in the front, an expanding shell following the core, and five observable filaments inside the shell. All the structures remain through the rest of the interaction. Interestingly, filamentation allows the pairs to maintain a high center density despite fast expansion of the shell.

Filamentation of plasmas could arise from or be influenced by two-stream instability, Weibel instability [38–40], or ponderomotive filamentation instability [34,41]. Although the formation of pair filamentation is correlated to counterpropagating pair streams, we cannot directly attribute the filamentation to the plasma streaming instability. The streaming instability exists in plasmas when counterpropagating streams carry a longitudinal current and a "return current" which produces strong transverse magnetic field to focus the streams [42–44]. However, the electron positron pairs respond symmetrically to the longitudinal laser pressure, including both the radiation reaction and the laser ponderomotive force. The longitudinally flowing pair streams are charge neutral and current neutral, at least in the center, and cannot produce a current or a "return current." Thus, the laser ponderomotive force is not likely to produce streaming instabilities of pair plasmas. In the specific simulation, the filaments grow and saturate within ten laser cycles. It is much shorter than the time scales [38,39] of two-stream instability $\tau_{\rm TS} \sim \gamma/\omega_p \sim 2300/\omega_0$ or the Weibel instability $\tau_{\rm W} \sim \sqrt{\gamma}/\omega_p \sim 95/\omega_0$, where ω_0 is the laser frequency.

More details of the filamentation process are shown in the pair momentum space in Fig. 3. The transverse momentum distribution p_y, plotted in the left column, reveals the pair oscillation in the laser field. Interestingly, the distribution in p_y shows narrow width compared to the maximum momentum. This can be explained from the factor that the creation and deceleration of pairs are synchronized with the peak laser amplitude, and their initial transverse momentum is negligible. The conservation of canonical momentum $p_y + a_0 m_e c$ leads to synchronized oscillation of p_y.

The right column of Fig. 3 show the longitudinal momentum distributions between 0.16 ps and 0.2 ps. The pairs start with unidirectional propagation in the $+x$ direction at $t = 0.16$ ps, illustrated in Fig. 3(a). They begin to show negative longitudinal momenta before $t = 0.18$ ps in Fig. 3(d), indicating partial pair reflection in the region near $x = 0$. It corresponds to the cavitation of pair sphere in Figs. 2(a) and 2(b). The distribution, however, does not show bump-on-tail distribution, which eliminates the possibility of two-stream instability.

To rule out the onset of Weibel instability, we next present the magnetic field profile in the $y = 0$ cross section in Fig. 4. Indeed, the transverse component B_y does not show filament structures. However, filament structures are observed in the longitudinal field B_x. They also manifest in the decrease of laser field amplitude B_z in the regions of pair filaments. Note that the background fields B_x and B_z extending between $z = -10\,\mu$m and $z = 10\,\mu$m are the intrinsic laser field [45], and more details can be found in the Appendix.

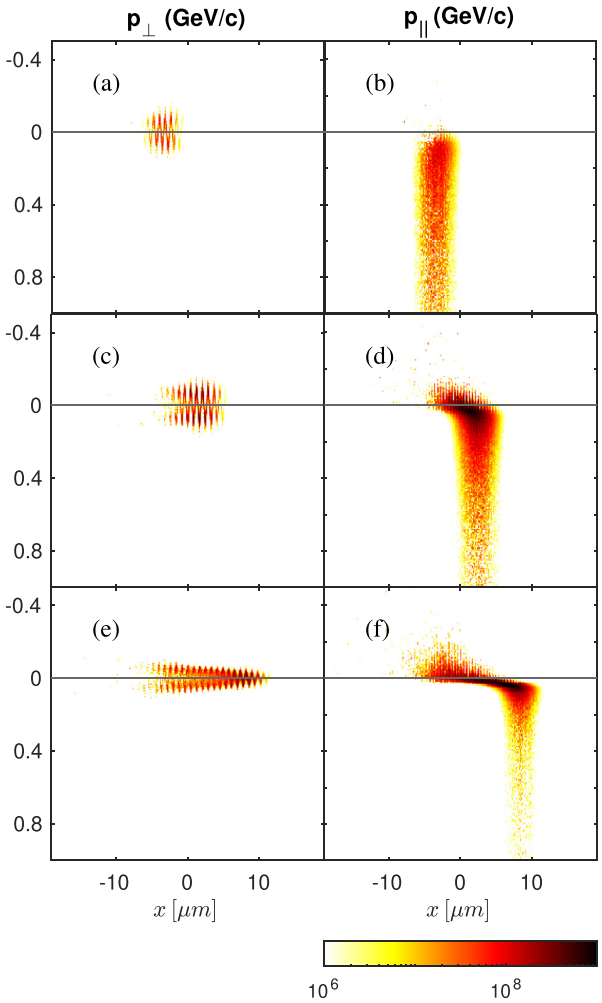

FIG. 3. Pair momentum distributions in the transverse direction (left column) and longitudinal direction (right column) at $t = 0.16$ ps (a), (b), 0.18 ps (c), (d), and 0.2 ps (e), (f), respectively.

The decrease of the B_z field in the region of pair filaments is an indication of ponderomotive filamentation [35], which is supported by two main features of the pair filamentation process illustrated in Fig. 2. First, the formation of filaments is strongly associated with its interaction with the laser field rather than a counterpropagating plasma. As seen in Figs. 2(c) and 2(d), the forward moving plasma shell and backward moving fringes do not overlap when the fringes condensate to filaments.

Second, the filaments exhibit higher contrast in the z direction, which is perpendicular to the laser polarization direction. The anisotropic filamentation is associated with Thomson scattering of the linearly polarized laser when the pair plasma dimension is smaller than the laser wavelength. The laser drives fundamental pair oscillation in the polarized direction $\hat{y}$ and second harmonic oscillation in the longitudinal direction $\hat{x}$. But only the fundamental mode beats with the input laser and it emits most strongly in the orthogonal trans-

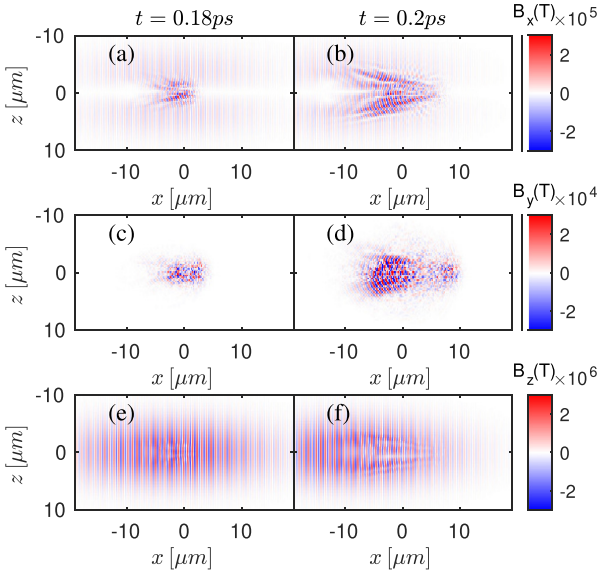

FIG. 4. Magnetic field B_x (a), (b), B_y (c), (d), and B_z (e), (f) in the $y = 0$ cross section at $t = 0.18$ ps (left column), and 0.2 ps (right column), respectively.

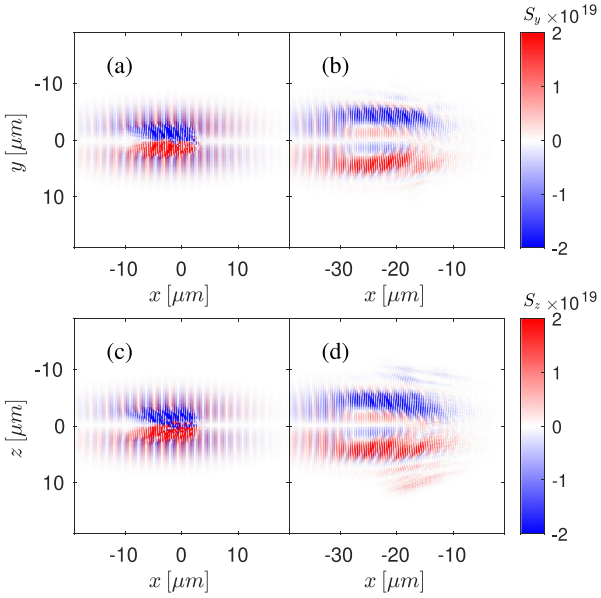

FIG. 5. Poynting vector (in unit Wm^{-2}) S_y in the $z = 0$ cross section (a), (b) and S_z in the $y = 0$ cross section (c), (d) at $t = 0.18$ ps (a), (c), and 0.26 ps (b), (d), respectively.

verse direction $\hat{z}$. Thus, fringes in the polarization direction $\hat{y}$ are suppressed. Laser scattering in the $\hat{y}$ direction only becomes strong when the plasma volume reaches near the laser wavelength and the scattering becomes Mie scattering. Mie scattering has a weak dependence on polarization but still has a strong dependence on the scattering angle. The anisotropic laser scattering serves as a seed for the quickly growing pair filamentation. The laser ponderomotive force pushes the plasma to regions of lower laser intensity, evident in Figs. 2(e) and 2(f). The plasma density inhomogeneity refracts the laser to regions with lower density and hence leads to filamentation instability.

Mie scattering of the laser can be visualized using the Poynting vectors plotted in Fig. 5. As soon as pair plasma is formed at $t = 0.18$ ps, the Poynting vectors in Figs. 5(a) and 5(c) show divergences in both transverse directions $\hat{y}$ and $\hat{z}$. As the filamented pairs copropagate with the laser, they continuously diffract the wave which, shown in Figs. 5(b) and 5(d), deviates from the laser pulse. Each panel of Fig. 5 also shows a low amplitude S beyond the region of the filaments. They illustrate the transverse energy outflow of the Gaussian laser pulse $S_r \propto |E|^2 r/R(x)$ where $R(x)$ is the radius of curvature of the beam at x. Compared to the background Poynting vector for the input laser (more details can be found in the Appendix), the diffraction modes are an order of magnitude stronger. The diffraction modes exhibit filament structure mainly in the $x - z$ plane, signifying the role of polarization of Thomson scattering.

III. LASER ENERGY SCATTERING

The pair filamentation has important implications to the QED cascade. It focuses the pairs in a few filaments of diameters similar to the laser wavelength, which otherwise expand continuously due to transverse laser ponderomotive force. The small filaments cause scattering of laser to large angles. Because the filaments are formed in the region of maximum laser intensity, they induce scattering of the laser energy which can be observed in the tail of the laser in Fig. 1 and in Figs. 5(b) and 5(d). More clearly, the peak laser intensity, illustrated as a blue solid curve in Fig. 6, shows a 40% decrease during the pair reflection between $t = 0.18$ ps and 0.2 ps. The figure also presents the total laser energy $\mathcal{E} = (\epsilon_0 E^2 + B^2/\mu_0)/2$ as a red dashed curve, which shows only a 0.3% decrease due to driving the pair oscillation and reflecting the pairs. Here ϵ_0 and μ_0 are the vacuum permittivity and permeability, respectively. Thus, the significant drop in peak laser intensity combined with approximately constant pulse energy comports with the theory of laser energy scattering.

The process of laser scattering is closely related to the laser frequency upshift when the mediating plasmas change

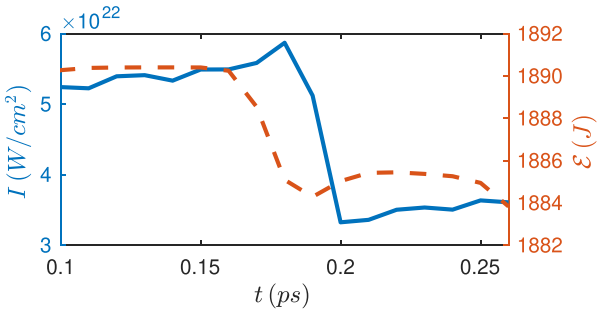

FIG. 6. Evolution of the peak laser intensity (blue solid) and total energy (red dashed).

density or Lorentz factor. In the problem of laser frequency upshift, the plasma is assumed homogeneous in the transverse direction. The transverse current thus strictly emits in the laser propagation direction or antiparallel to it. The emission couples to the original laser field to cause laser frequency upshift. However, pair filamentation breaks the symmetry and the oscillating pairs emit to the whole space due to finite current dimension.

We can analytically estimate the rate of laser intensity decrease. The transverse current carried by the created pairs is

$$\boldsymbol{J} = \int_0^t dt' \frac{2\partial n_p}{\partial t'} \int_{t'}^t \frac{e^2}{\gamma(t'')m_e} \boldsymbol{E}(t'')dt'' = \frac{2e^2}{m_e} \int_0^t \frac{n_p \boldsymbol{E}}{\gamma} dt'. \quad (1)$$

We only consider the current oscillating at the laser frequency ω because the resonance causes nonreciprocating laser energy scattering. The pair density n_p is dependent on both time and space. In the beginning of QED cascade, n_p can be modeled as a δ function in space. Because the pairs oscillate synchronously, they behave as a relativistic dipole to induce Thomson scattering.[1] The angle dependence of the scattered light changes from $\sin^2\theta_1$ at $\gamma \sim 0$ to $[(1-\cos\theta_2)^2 - \sin^2\theta_2\cos^2\phi/\gamma^2]/(1-\cos\theta_2)^5$ at $\gamma \gg 1$, where θ_1 and θ_2 are the angles between the scattered light and the laser polarization direction $\hat{y}$ and the laser propagation direction $\hat{x}$, and ϕ is the angle between $\hat{y}$ and the plane of the scattering direction and $\hat{x}$. When the pair volume grows to the scale of λ^3, the scattering needs to be described by the Mie theory. It is strongly dependent on the scattering angle and requires numerical treatment. But because both Thomson scattering and Mie scattering are anisotropic, the scattered light beats with the input laser to cause filamentation of the pair plasmas.

According to the Poynting theorem, the decrease of laser energy density U is described with $dU/dt = -\nabla\cdot\boldsymbol{S} - \boldsymbol{J}\cdot\boldsymbol{E}$, where $U \equiv \epsilon_0|E|^2$ in dispersive media. Note, however, that because Poynting flux $\boldsymbol{S}$ of the scattering arises from the emission of the transverse current $\boldsymbol{J}$, the decrease of energy density U can be found by analyzing the term $\boldsymbol{J}\cdot\boldsymbol{E}$. We describe the laser field as $\boldsymbol{E} = \boldsymbol{E}_0\cos\varphi$ and the pair density as $n_p = n_p\Theta(\varphi-\varphi_0)$, where $\varphi = \omega t - \boldsymbol{k}x$ and $\varphi_0 = 0$ is the instant of pair stopping at the laser peak. The transverse current can be expressed as $\boldsymbol{J} \cong 2\epsilon_0\omega n_p\boldsymbol{E}_0\sin\varphi\Theta(\varphi-\varphi_0)/(n_c\gamma)$, where n_c is the critical density of frequency ω. Thus, the laser energy density decreases as

$$\frac{dU}{d\varphi} = -\frac{2\epsilon_0 n_p}{\gamma n_c} E_0^2 \sin\varphi\cos\varphi\Theta(\varphi-\varphi_0). \quad (2)$$

The differential equation shows that energy is transferred from the laser to the transverse current when $0 < \varphi < \pi/2$ and is transferred back to the wave when $\pi/2 < \varphi < \pi$. But the latter process radiates to the whole space and hence, its contribution to the input laser pulse can be neglected. Therefore, the decrease of peak laser energy density near the pair stopping point can be found by taking the average of $dU/d\varphi$ in half a cycle

$$\left\langle \frac{dU}{d\varphi} \right\rangle = -\frac{n_p}{\gamma n_c}\langle U\rangle. \quad (3)$$

The result shows that the laser energy decreases exponentially at a rate dependent on the effective plasma density n_p/γ. For the presented simulation, the pair plasma has a length of $\sim 12\lambda$ with $n_p/(\gamma n_c) \sim 6.7\%$. It results in a laser energy density decrease of $\sim 50\%$, which agrees well with simulation results. Note that the frequency upshift process in a strict 1D scenario also causes a decrease of laser energy density, but the decrease scales with $1/\omega$ which is an order of magnitude lower than 40% in the simulation.

IV. CONCLUSIONS AND DISCUSSIONS

In conclusion, we investigate the formation of pair filamentation in an electron-beam-driven QED cascade through a 3D QED PIC simulation. The pair filamentation is observed in the "pair reflection" regime, in which an above-threshold laser decelerates the pair plasmas and reverts their propagation direction. The simulation reveals the development of pair filaments in the longitudinal direction when the laser traverses through the pair plasma. Using a linearly polarized laser, we observe that the pair density first exhibits periodic modulation in the plane perpendicular to the polarization direction. Within a few laser cycles, the density modulation condenses into filaments with a diameter similar to the laser wavelength. Importantly, this timescale extends beyond that of streaming instabilities. Furthermore, considering the absence of a robust transverse magnetic field perpendicular to the laser, we dismiss the possibility of two-stream instability or Weibel instability in this scenario.

We attribute the origin of pair filamentation to the laser ponderomotive force. The initially small pair plasma induces highly anisotropic scattering of the laser, creating interference patterns with the incident laser and establishing a pressure gradient within the pair plasma. Pairs are expelled from regions of high laser intensity, and pair cavitation gives rise to locally elevated refractive indices that focus the laser pulse. The inhomogeneous plasma density also contributes to the refraction of laser energy. Consequently, filamentation takes shape in the region where dense pair plasma is stopped. As the reflected pairs and the laser pulse copropagate, their slippage is diminished, facilitating the rapid growth of pair filaments. This reduced slippage enables efficient coupling between the reflected pairs and the laser pulse, augmenting the development of pair filaments in this dynamic interplay.

Laser polarization critically influences the formation of pair plasma filamentation. In the initial stage of interaction, the small plasma oscillates synchronously to cause stronger scattering in the direction perpendicular to the polarization direction. Because the scattering is negligible in the polarization direction, a linearly polarized laser only creates 2D gratings in the initial stage when the pair plasma is smaller than the laser wavelength. As the plasma volume grows, the scattering becomes less polarization dependent.

[1]The scattering is inelastic because we focus on photon emissions with the same frequency which can only beat with the input laser to create the intensity fringes.

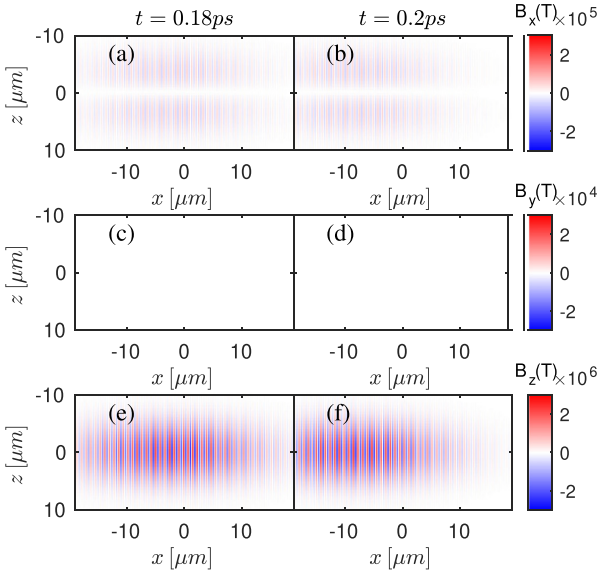

FIG. 7. The laser magnetic field B_x (a), (b), B_y (c), (d), and B_z (e), (f) in the $y = 0$ cross section without interacting with electron beam at $t = 0.18$ ps (left column), and 0.2 ps (right column), respectively.

The rapidly expanding plasma volume in the beam-driven QED cascade sets itself apart from ponderomotive filamentation observed when a low-intensity laser traverses stationary plasmas. In the QED cascade, the small pair plasma does not only directly seed the filamentation, but also accentuates the instability through causing Mie scattering. The beat

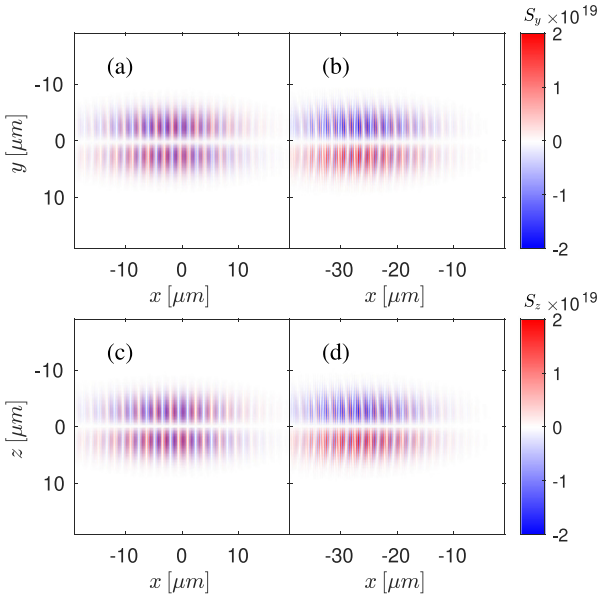

FIG. 8. Poynting vector (in unit Wm^{-2}) S_y in the $z = 0$ cross section (a), (b) and S_z in the $y = 0$ cross section (c), (d) of the laser without interacting with electron beam at $t = 0.18$ ps (a), (c), and 0.26 ps (b), (d), respectively.

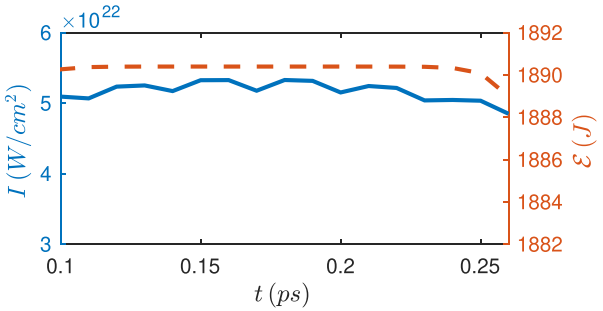

FIG. 9. Evolution of the peak laser intensity (blue solid) and total energy (red dashed).

of the scattered light and input laser leads to strong modulation of pair density. A full analytical model that describes the coupling requires carefully treating both ultrarelativistic particle motion and also complicated Mie scattering in multidimensions. Thus, the filamentation growth rate of the pair plasma significantly deviates from known expressions of the ponderomotive filamentation instability [34].

The pair filamentation has important implications to the joint problem of creating and observing QED plasmas. First, filamentation focuses pairs and creates high pair density regions inside the laser field. Compared to homogeneously distributed pairs, filamentation reduces the total pair number needed to reach high pair density. Second, despite being highly localized, the dense pair plasma interacts with the most intense part of the laser. The strong scattering of laser energy due to small filament dimensions causes a dramatic decrease in laser intensity within the filament length. All the scattered laser energy is redistributed and can be detected at large angles. Because the scattering arises from the interaction of collective pair motion and the laser fields, it serves as one more signature of QED plasma effect.

ACKNOWLEDGMENT

This work was supported by NSF Grant No. PHY-2206691.

APPENDIX

The linearly polarized Gaussian laser pulse contains fields in multiple directions due to its finite waist size, $w_0 = 5\,\mu$m. With its electric field polarized in the y -direction, the electric and magnetic fields in vacuum can be written to the second order of $(w_0/z_R) \approx 0.05$ as [45]

$$E_x = \tilde{E}\frac{y}{z_R}\frac{w_0}{w(x)}\cos(\varphi + 2\varphi_G - \varphi_R), \tag{A1}$$

$$E_y = \tilde{E}\left\{\sin(\varphi + \varphi_G) + \frac{w_0^2}{z_R^2}\left[\frac{y^2}{w^2(x)}\sin(\varphi + 3\varphi_G) - \frac{(y^2+z^2)^2}{4w_0 w^3(x)}\sin(\varphi + 4\varphi_G)\right]\right\}, \tag{A2}$$

$$E_z = \tilde{E}\frac{yz}{z_R^2}\frac{w_0^2}{w^2(x)}\sin(\varphi + 3\varphi_G), \tag{A3}$$

$$B_x = \frac{\tilde{E}}{c}\frac{z}{z_R}\frac{w_0}{w(x)}\cos(\varphi + 2\varphi_G), \tag{A4}$$

$$B_y = 0, \tag{A5}$$

$$B_z = \frac{\tilde{E}}{c}\left\{\sin(\varphi+\varphi_G) + \frac{w_0^2}{z_R^2}\left[\frac{y^2+z^2}{2w^2(x)}\sin(\varphi+3\varphi_G) - \frac{(y^2+z^2)^2}{4w_0 w^3(x)}\sin(\varphi+4\varphi_G)\right]\right\}, \tag{A6}$$

where $k=-2\pi/\lambda$, $w(x)=w_0\sqrt{1+(x/x_R)^2}$ is the spot size at distance x, $\varphi=\omega t-kx-k(y^2+z^2)/(2R)$, $R=x+x_R^2/x$, $\varphi_G=-\arctan(x/x_R)$ is the Gouy phase, and $\tilde{E}=E_0[w_0/w(x)]\exp[-(y^2+z^2)/w^2(x)]\exp[-(t-x/c)^2/\tau^2]$ is the envelope of the Gaussian beam, with $\tau=50$ fs.

Figure 7 shows the magnetic fields of laser in vacuum for direct comparison with Fig. 4.

Figure 8 shows the Poynting vectors of laser in vacuum for direct comparison with Fig. 5. The decrease of energy at $t=0.26$ ps is caused by laser exiting the simulation window.

Figure 9 shows the evolution of the peak laser intensity and total energy in vacuum for direct comparison with Fig. 6.

[1] C. N. Danson, C. Haefner, J. Bromage, T. Butcher, J.-C. F. Chanteloup, E. A. Chowdhury, A. Galvanauskas, L. A. Gizzi, J. Hein, D. I. Hillier *et al.*, Petawatt and exawatt class lasers worldwide, High Power Laser Sci. Eng. **7**, e54 (2019).

[2] E. Cartlidge, The light fantastic, Science **359**, 382 (2018).

[3] C. Radier, O. Chalus, M. Charbonneau, S. Thambirajah, G. Deschamps, S. David, J. Barbe, E. Etter, G. Matras, S. Ricaud *et al.*, 10 PW peak power femtosecond laser pulses at ELI-NP, High Power Laser Sci. Eng. **10**, e21 (2022).

[4] V. I. Ritus, Quantum effects of the interaction of elementary particles with an intense electromagnetic field, J. Sov. Laser Res. **6**, 497 (1985).

[5] T. Erber, High-energy electromagnetic conversion processes in intense magnetic fields, Rev. Mod. Phys. **38**, 626 (1966).

[6] A. Di Piazza, C. Müller, K. Z. Hatsagortsyan, and C. H. Keitel, Extremely high-intensity laser interactions with fundamental quantum systems, Rev. Mod. Phys. **84**, 1177 (2012).

[7] A. R. Bell and J. G. Kirk, Possibility of prolific pair production with high-power lasers, Phys. Rev. Lett. **101**, 200403 (2008).

[8] I. V. Sokolov, N. M. Naumova, J. A. Nees, and G. A. Mourou, Pair creation in QED-strong pulsed laser fields interacting with electron beams, Phys. Rev. Lett. **105**, 195005 (2010).

[9] M. Jirka, O. Klimo, S. V. Bulanov, T. Z. Esirkepov, E. Gelfer, S. S. Bulanov, S. Weber, and G. Korn, Electron dynamics and γ and e^-e^+ production by colliding laser pulses, Phys. Rev. E **93**, 023207 (2016).

[10] G. Sarri, K. Poder, J. M. Cole, W. Schumaker, A. Di Piazza, B. Reville, T. Dzelzainis, D. Doria, L. A. Gizzi, G. Grittani, S. Kar, C. H. Keitel, K. Krushelnick, S. Kuschel, S. P. D. Mangles, Z. Najmudin, N. Shukla, L. O. Silva, D. Symes, A. G. R. Thomas *et al.*, Generation of neutral and high-density electron-positron pair plasmas in the laboratory, Nat. Commun. **6**, 6747 (2015).

[11] X.-L. Zhu, T.-P. Yu, Z.-M. Sheng, Y. Yin, I. C. E. Turcu, and A. Pukhov, Dense GeV electron–positron pairs generated by lasers in near-critical-density plasmas, Nat. Commun. **7**, 1 (2016).

[12] T. Grismayer, M. Vranic, J. L. Martins, R. A. Fonseca, and L. O. Silva, Seeded QED cascades in counterpropagating laser pulses, Phys. Rev. E **95**, 023210 (2017).

[13] M. Lobet, X. Davoine, E. d'Humières, and L. Gremillet, Generation of high-energy electron-positron pairs in the collision of a laser-accelerated electron beam with a multipetawatt laser, Phys. Rev. Accel. Beams **20**, 043401 (2017).

[14] D. Del Sorbo, L. Antonelli, P. J. Davies, L. N. K. Döhl, C. D. Murphy, N. Woolsey, F. Fiuza, H. Chen, and C. P. Ridgers, A channel for very high density matter-antimatter pair-jet production by intense laser-pulses, arXiv:1902.01044.

[15] D. L. Burke, R. C. Field, G. Horton-Smith, J. E. Spencer, D. Walz, S. C. Berridge, W. M. Bugg, K. Shmakov, A. W. Weidemann, C. Bula, K. T. McDonald, E. J. Prebys, C. Bamber, S. J. Boege, T. Koffas *et al.*, Positron production in multiphoton light-by-light scattering, Phys. Rev. Lett. **79**, 1626 (1997).

[16] C. Bamber, S. J. Boege, T. Koffas, T. Kotseroglou, A. C. Melissinos, D. D. Meyerhofer, D. A. Reis, W. Ragg, C. Bula, K. T. McDonald, E. J. Prebys, D. L. Burke, R. C. Field, G. Horton-Smith, J. E. Spencer *et al.*, Studies of nonlinear QED in collisions of 46.6 GeV electrons with intense laser pulses, Phys. Rev. D **60**, 092004 (1999).

[17] K. Poder, M. Tamburini, G. Sarri, A. Di Piazza, S. Kuschel, C. D. Baird, K. Behm, S. Bohlen, J. M. Cole, D. J. Corvan, M. Duff, E. Gerstmayr, C. H. Keitel, K. Krushelnick, S. P. D. Mangles, P. McKenna, C. D. Murphy, Z. Najmudin, C. P. Ridgers, G. M. Samarin *et al.*, Experimental signatures of the quantum nature of radiation reaction in the field of an ultraintense laser, Phys. Rev. X **8**, 031004 (2018).

[18] J. M. Cole, K. T. Behm, E. Gerstmayr, T. G. Blackburn, J. C. Wood, C. D. Baird, M. J. Duff, C. Harvey, A. Ilderton, A. S. Joglekar, K. Krushelnick, S. Kuschel, M. Marklund, P. McKenna, C. D. Murphy, K. Poder, C. P. Ridgers, G. M. Samarin, G. Sarri, D. R. Symes *et al.*, Experimental evidence of radiation reaction in the collision of a high-intensity laser pulse with a laser-wakefield accelerated electron beam, Phys. Rev. X **8**, 011020 (2018).

[19] H. Chen and F. Fiuza, Perspectives on relativistic electron–positron pair plasma experiments of astrophysical relevance using high-power lasers, Phys. Plasmas **30**, 020601 (2023).

[20] P. Zhang, S. S. Bulanov, D. Seipt, A. V. Arefiev, and A. G. R. Thomas, Relativistic plasma physics in supercritical fields, Phys. Plasmas **27**, 050601 (2020).

[21] S. Meuren, D. A. Reis, R. Blandford, P. H. Bucksbaum, N. J. Fisch, F. Fiuza, E. Gerstmayr, S. Glenzer, M. J. Hogan, C. Pellegrini, M. E. Peskin, K. Qu, G. White, and V. Yakimenko, MP3 white paper 2021 – research opportunities enabled by co-locating multi-petawatt lasers with dense ultra-relativistic electron beams, arXiv:2105.11607.

[22] S. Meuren, P. H. Bucksbaum, N. J. Fisch, F. Fiúza, S. Glenzer, M. J. Hogan, K. Qu, D. A. Reis, G. White, and V. Yakimenko, On seminal hedp research opportunities enabled by

colocating multi-petawatt laser with high-density electron beams, arXiv:2002.10051.
[23] K. Qu, S. Meuren, and N. J. Fisch, Signature of collective plasma effects in beam-driven QED cascades, Phys. Rev. Lett. **127**, 095001 (2021).
[24] K. Qu, S. Meuren, and N. J. Fisch, Collective plasma effects of electron–positron pairs in beam-driven QED cascades, Phys. Plasmas **29**, 042117 (2022).
[25] S. S. Bulanov, A. M. Fedotov, and F. Pegoraro, Damping of electromagnetic waves due to electron-positron pair production, Phys. Rev. E **71**, 016404 (2005).
[26] A. Griffith, K. Qu, and N. J. Fisch, Particle deceleration for collective QED signatures, Phys. Plasmas **29**, 073104 (2022).
[27] K. Qu, S. Meuren, and N. J. Fisch, Creating pair plasmas with observable collective effects, Plasma Phys. Control. Fusion **65**, 034007 (2023).
[28] A. Griffith, K. Qu, and N. J. Fisch, Radiation reaction kinetics and collective QED signatures, arXiv:2312.04700.
[29] E. V. Stenson, J. Horn-Stanja, M. R. Stoneking, and T. S. Pedersen, Debye length and plasma skin depth: two length scales of interest in the creation and diagnosis of laboratory pair plasmas, J. Plasma Phys. **83**, 595830106 (2017).
[30] C. J. Joshi, C. E. Clayton, K. Marsh, D. B. Hopkins, A. Sessler, and D. Whittum, Demonstration of the frequency upshifting of microwave radiation by rapid plasma creation, IEEE Trans. Plasma Sci. **18**, 814 (1990).
[31] S. C. Wilks, J. M. Dawson, and W. B. Mori, Frequency up-conversion of electromagnetic radiation with use of an overdense plasma, Phys. Rev. Lett. **61**, 337 (1988).
[32] J. T. Mendonça, *Theory of Photon Acceleration* (Institute of Physics Publishing, wholly owned by The Institute of Physics, London, 2000).
[33] K. Qu, Q. Jia, M. R. Edwards, and N. J. Fisch, Theory of electromagnetic wave frequency upconversion in dynamic media, Phys. Rev. E **98**, 023202 (2018).
[34] W. L. Kruer, Ponderomotive and thermal filamentation of laser light, Comments Plasma Phys. Control. Fusion **9**, 63 (1985).
[35] P. Kaw, G. Schmidt, and T. Wilcox, Filamentation and trapping of electromagnetic radiation in plasmas, Phys. Fluids **16**, 1522 (1973).
[36] P. E. Young, H. A. Baldis, R. P. Drake, E. M. Campbell, and K. G. Estabrook, Direct evidence of ponderomotive filamentation in a laser-produced plasma, Phys. Rev. Lett. **61**, 2336 (1988).
[37] E. Sobacchi, Y. Lyubarsky, A. M. Beloborodov, L. Sironi, and M. Iwamoto, Saturation of the filamentation instability and dispersion measure of fast radio bursts, Astrophys. J. Lett. **943**, L21 (2023).
[38] A. Bret, M.-C. Firpo, and C. Deutsch, Collective electromagnetic modes for beam-plasma interaction in the whole k space, Phys. Rev. E **70**, 046401 (2004).
[39] A. Bret, M.-C. Firpo, and C. Deutsch, Characterization of the initial filamentation of a relativistic electron beam passing through a plasma, Phys. Rev. Lett. **94**, 115002 (2005).
[40] M. D'Angelo, L. Fedeli, A. Sgattoni, F. Pegoraro, and A. Macchi, Particle acceleration and radiation friction effects in the filamentation instability of pair plasmas, Mon. Not. R. Astron. Soc **451**, 3460 (2015).
[41] E. M. Epperlein, Kinetic theory of laser filamentation in plasmas, Phys. Rev. Lett. **65**, 2145 (1990).
[42] E. S. Weibel, Spontaneously growing transverse waves in a plasma due to an anisotropic velocity distribution, Phys. Rev. Lett. **2**, 83 (1959).
[43] E. G. Harris, Unstable plasma oscillations in a magnetic field, Phys. Rev. Lett. **2**, 34 (1959).
[44] B. D. Fried, Mechanism for instability of transverse plasma waves, Phys. Fluids **2**, 337 (1959).
[45] Y. I. Salamin, G. R. Mocken, and C. H. Keitel, Electron scattering and acceleration by a tightly focused laser beam, Phys. Rev. ST Accel. Beams **5**, 101301 (2002).